TET1 non-catalytic activity shapes the chromatin landscape that directs de novo methylation establishment in the male germline

Prasasya, R. D.[1], Kim, J. J.[1], Liu, Z.[1], Kohli, R. M.[2,3], Bartolomei, M. S.[1,3]

[1]Department of Cell and Developmental Biology, Perelman School of Medicine, University of Pennsylvania, Philadelphia, PA 19104, USA

[2]Department of Medicine, Perelman School of Medicine, University of Pennsylvania, Philadelphia, PA 19104, USA

[3]Penn Epigenetics Institute, University of Pennsylvania, Philadelphia, PA, 19104, USA

*Correspondence: bartolom@pennmedicine.upenn.edu (MSB)

Abstract

In the germline, DNA methylation is globally erased in primordial germ cells (PGCs), enabling establishment of sex-specific methylomes in prospermatogonia or oocytes. The catalytic activity of TET1 is required for complete demethylation in PGCs, yet sperm from *Tet1*$^{-/-}$ mice display methylation defects not explained by incomplete erasure. Instead, these defects arise from abnormal *de novo* methylation during development, coinciding with erosion of H3K4me3, a chromatin modification that blocks DNMT3A/3L. Using a catalytically inactive *Tet1*^{HxD} mouse line, we demonstrate a non-catalytic role of TET1 in promoting H3K4me3 deposition and protecting a subset of sperm hypomethylated regions from aberrant methylation in prospermatogonia.

23 **Introduction**

24 DNA methylation is one of the most sexually dimorphic epigenetic marks in mammalian
25 gametes (Stewart et al. 2016). Following specification from cells of the proximal epiblast,
26 primordial germ cells (PGCs) undergo epigenetic reprogramming that involves both chromatin
27 remodeling and genome-wide DNA methylation erasure (Saitou et al. 2005; Smith and Meissner
28 2013; Saitou et al. 2011). In the mouse developmental timeline, the PGC genome attains a
29 hypomethylated state by embryonic day (E)13.5 (Seisenberger et al. 2012). From this common
30 basal epigenetic state, the sperm genome becomes highly methylated (~90% overall
31 methylation in the mouse) while the oocyte genome remains intermediate, with distinct hyper-
32 and hypomethylated domains (Kobayashi et al. 2012; Hanna et al. 2018). In the male germline,
33 acquisition of DNA methylation occurs in prospermatogonia between E15.5 and postnatal day 0.
34 In contrast, *de novo* methylation occurs postnatally in oocytes when individual follicles are
35 recruited for growth during each estrus cycle. Despite the distinct timing and the divergent
36 resulting methylomes between the two sexes, *de novo* DNA methylation is facilitated by a
37 common DNA methyltransferase (DNMT) complex: DNMT3A and its noncatalytic co-factor
38 DNMT3L (DNMT3A/3L) (Kaneda et al. 2004; Kato et al. 2007; Bourc'his and Bestor 2004).

39 The mechanisms that target DNMT3A/3L to distinct loci in prospermatogonia versus the
40 growing oocyte to generate sex-specific methylomes are still unclear. Biochemical studies
41 suggest crosstalk between histone post-translational modifications (PTMs) and genome
42 accessibility for DNMT3A/3L. For example, the PWWP domain of DNMT3A binds to di- or tri-
43 methylated H3K36 (H3K36me2/me3) (Dhayalan et al. 2010). In the germline, H3K36me2
44 enriched domains are highly correlated with DNA methylation acquisition in prospermatogonia
45 while transcription-coupled H3K36me3 deposition directs DNA methylation in the oocyte
46 (Shirane et al. 2020; Chotalia et al. 2009; Stewart et al. 2015). In contrast, methylation of H3K4
47 (H3K4me1/2/3) repels the ADD domain of DNMT3A and DNMT3L, inhibiting DNA methylation
48 activity (Zhang et al. 2010; Ooi et al. 2007). Consequently, H3K4me3 remodeling is required for

49 proper DNA methylation acquisition in the oocyte (Hanna et al. 2018). In the male germline,
50 DNA methylation acquisition occurs broadly, except at regions enriched for H3K4me2 at the
51 prospermatogonia stage (Singh et al. 2013) . Our previous data also confirmed the high
52 congruency of H3K4me3 enrichment in prospermatogonia with sperm hypomethylated regions
53 (HMRs) (Prasasya et al. 2024). To date, however, how the genome is patterned for
54 H3K36me2/3 or H3K4me1/2/3 prior to gametic *de novo* methylation establishment remains
55 unresolved.

56 In our previous investigation of the methylcytosine dioxygenase, Tet-eleven translocation
57 1 (TET1), in germline reprogramming, we described extensive methylation defects in *Tet1*$^{-/-}$
58 sperm beyond the previously described limited numbers of TET1-dependent loci (i.e. imprinting
59 control regions -ICRs- and meiosis-associated gene promoters that require TET1 during PGC
60 epigenetic reprogramming) (Prasasya et al. 2024; Yamaguchi et al. 2012, 2013; Hill et al. 2018;
61 SanMiguel et al. 2018). TET enzymes iteratively oxidize 5-methylcytosine (5mC) to 5-
62 hydroxymethylcytosine (5hmC), 5-formylcytosine (5fC), and 5-carboxylcytosine (5caC) (Ito et al.
63 2011). 5hmC is poorly recognized by maintenance DNMT1, while 5fC and 5caC can be excised
64 by thymine DNA glycosylase (TDG) resulting in an abasic site, activating the base excision
65 repair machinery to recover unmodified cytosine (Kohli and Zhang 2013). Using mouse models
66 harboring 5hmC-stalling (diminished activity in generating 5fC/5caC) TET1^{V} and catalytically
67 inactive TET1^{HxD}, we established the necessity of TET1 iterative oxidative capability in germline
68 epigenetic reprogramming. Intriguingly, only a small portion of methylation defects observed in
69 *Tet1*$^{-/-}$ sperm can be attributed to the loss of TET1 catalytic activity. In fact, expression of full-
70 length, catalytically compromised TET1 (TET1^{HxD}) was sufficient to rescue about 2/3 of
71 methylation defects observed in *Tet1*$^{-/-}$ sperm (Prasasya et al. 2024). In addition to the catalytic
72 core located within the C-terminus, TET proteins possess an extensive N-terminus with the
73 ability to interact with and recruit several histone modifiers such as OGT, Sin3a, and PRC2 *in*
74 *vivo* (Vella et al. 2013; Zhu et al. 2018; Wu et al. 2011; Chrysanthou et al. 2022). Here, we

75 demonstrate that the majority of hypermethylation in *Tet1*$^{-/-}$ sperm arises from abnormal *de novo*
76 methylation and coincides with diminished H3K4me3 at intergenic hypomethylated regions.
77 Importantly, catalytically inactive TET1 was sufficient to restore H3K4me3, establishing a non-
78 catalytic role for TET1 in shaping the chromatin landscape of the male germline.
79
80 **Results and Discussion**
81 We conducted global DNA methylation analysis of *Tet1*$^{-/-}$ and WT (*Tet1*$^{+/+}$) PGCs at the
82 completion of reprogramming, E13.5, using the mouse Illumina Infinium Methylation BeadChip.
83 Consistent with previous reports, the *Tet1*$^{-/-}$ PGC genome was not globally hypermethylated
84 compared to WT (Supplemental Fig. 1A) (Yamaguchi et al. 2013; Hill et al. 2018). Aberrantly
85 methylated regions in *Tet1*$^{-/-}$ PGCs were almost exclusively hypermethylated and enriched for
86 ICRs (Figure 1A, Supplemental Fig. 1B, Supplemental Table S1A; 1049 hypermethylated
87 differentially methylated regions -DMRs-, 1 hypomethylated DMR; each DMR corresponds to a
88 single probe on the array). Gene ontology (GO) analysis revealed that hypermethylated DMRs
89 were enriched for genes involved in meiosis prophase I (Figure 1B), consistent with previous
90 findings by us and others showing that promoter activation requires proper demethylation (Hill et
91 al. 2018; Prasasya et al. 2024). We compared hypermethylated DMRs in *Tet1*$^{-/-}$ PGCs with
92 differentially expressed genes (DEGs) from our previously described RNA-seq (Figure 1C)
93 (Prasasya et al. 2024). Only DMRs within promoters of meiosis-associated genes corresponded
94 to downregulated expression, suggesting that the transcriptional consequences of TET1-
95 dependent hypermethylation outside of these meiosis-associated genes may manifest later in
96 germ cell development.
97 To assess whether incomplete DNA methylation erasure during PGC development
98 explains the hypermethylation defects previously reported in *Tet1*$^{-/-}$ sperm (Prasasya et al.
99 2024), we compared hypermethylated DMRs at the two stages (Figure 1D-E, Supplemental
100 Table S1B). 348 DMRs were hypermethylated in both *Tet1*$^{-/-}$ PGCs and sperm. As shown in the

101 distribution plot (Figure 1E, panel iii, Supplemental Table S1E), average methylation levels of
102 these regions were unchanged between sperm and PGCs for both genotypes, suggesting that
103 only a small fraction (6.18%) of *Tet1*$^{-/-}$ sperm hypermethylation results from incomplete erasure
104 in PGCs. In contrast, the majority of hypermethylated DMRs in *Tet1*$^{-/-}$ sperm showed no change
105 in *Tet1*$^{-/-}$PGCs compared to WT (Figure 1E, panel i-ii), indicating replication-coupled passive
106 dilution of DNA methylation was sufficient to reprogram these loci. Instead, these regions
107 abnormally acquired DNA methylation following successful erasure in *Tet1*$^{-/-}$ germ cells (Figure
108 1E, panel i-ii, Supplemental Table S1C-D).

109 When comparing WT PGCs and sperm, we noted a subset of regions where DMRs
110 typically gain methylation during normal male germline development; in *Tet1*$^{-/-}$*,* this acquisition
111 was exaggerated, resembling a hypermorphic phenotype (Figure 1E, panel i). In contrast, a
112 second subset of regions typically remained unmethylated in WT sperm but ectopically gained
113 methylation in *Tet1*$^{-/-}$ (Figure 1E, panel ii). Out of the 5283 *Tet1*$^{-/-}$ sperm DMRs that originated
114 from abnormal methylation acquisition, the majority belonged to the category of hypermorphic
115 gain (3667 hypermorphic gain, 1602 ectopic gain, 14 sperm DMRs did not pass filter in the PGC
116 data set). Finally, we identified 701 regions that required TET1 for reprogramming in PGCs but
117 ultimately became fully methylated in both *Tet1*$^{-/-}$ and WT sperm (e.g. paternally methylated
118 ICRs such as *H19* or *IG-DMR*) or sperm HMRs that continued to demethylate as the germ cells
119 resumed mitosis in spermatogonial stem cells (SSCs) (Figure 1E, panel iv, Supplemental Table
120 S1F). Design group enrichment analysis showed that abnormal methylation gain with TET1 loss
121 occurred at enhancers and long noncoding RNA (lncRNA) promoters, whereas regions with
122 either incomplete erasure or exclusively hypermethylated in PGCs occurred mainly at ICRs
123 (Supplemental Fig. 1C–F). Overall, these findings suggest that TET1 not only supports
124 epigenetic reprogramming in PGCs but also regulates proper DNA methylation acquisition
125 during male germline development.

126 We hypothesized that abnormal gain of methylation observed in the *Tet1*$^{-/-}$ male
127 germline occurs concurrently with *de novo* methylation establishment and reflects changes in
128 the chromatin landscape in prospermatogonia. To test this, we conducted CUT&RUN for
129 H3K4me3, a histone PTM that inhibits DNMT3A/3L activity, in E17.5 prospermatogonia. We
130 chose E17.5 as a mid-point of global wave of *de novo* methylation that occurs between E15.5
131 and birth in the male germline (Kobayashi et al. 2013; Seisenberger et al. 2012; Singh et al.
132 2013). For both WT and *Tet1*$^{-/-}$, over 50% of identified peaks were located within distal
133 intergenic regions (Supplemental Fig. 2A). Most identified peaks showed overlap between *Tet1*$^{-}$
134 $^{/-}$ and WT prospermatogonia, although *Tet1*$^{-/-}$ prospermatogonia had fewer consensus peaks
135 compared to WT (67205 vs 95643 peaks; consensus peaks were defined as peaks called in at
136 least 2 out of 3 biological replicates; Supplemental Fig. 2A, B, Supplemental Table S2A, B).
137 Averaged signals across genic regions or intergenic peaks revealed distinct H3K4me3 changes
138 in *Tet1*$^{-/-}$ prospermatogonia (Figure 2A). While *Tet1*$^{-/-}$ prospermatogonia showed higher overall
139 H3K4me3 near transcriptional start sites (TSSs), H3K4me3 was markedly lower at intergenic
140 peaks (Figure 2A). Differential enrichment (FDR ≤ 0.05, minimum 1.5-fold change vs WT)
141 identified 22904 regions that lost H3K4me3, mostly intergenic regions, in *Tet1*$^{-/-}$
142 prospermatogonia (Supplemental Fig. 2D, Supplemental Table S3A). In contrast, 10971 regions
143 that gained H3K4me3 mapped predominantly within genic regions (Supplemental Fig. 2D,
144 Supplemental Table S3B). Notably, in prospermatogonia, intergenic H3K4me3 signal intensities
145 were comparable to those at TSSs (Figure 2A; Supplemental Fig. 2E-F), underscoring their
146 potential regulatory importance (Guenther et al. 2007) .

147 As we previously showed, H3K4me3 enrichment in prospermatogonia strongly
148 overlapped with sperm HMRs (Figure 2B, Supplemental Fig. 2C) (Prasasya et al. 2024). With
149 TET1 loss, we observed significantly less overlap (in absolute number of sperm HMRs) between
150 E17.5 H3K4me3 peaks and sperm HMRs (Figure 2B). This initial analysis suggested that fewer

151 sperm HMRs were protected by H3K4me3 in *Tet1*$^{-/-}$ prospermatogonia. To follow up, we
152 analyzed the relationship between *Tet1*$^{-/-}$ sperm DMRs and changes to H3K4me3 in *Tet1*$^{-/-}$
153 prospermatogonia. With the caveat that the Infinium array provided methylation data for only a
154 representative subset of the genome, we found strong overlap between regions that lost
155 H3K4me3 in *Tet1*$^{-/-}$ prospermatogonia and hypermethylated DMRs in *Tet1*$^{-/-}$ sperm (Figure 2C).
156 As described above, the majority of *Tet1*$^{-/-}$ sperm hypermethylated DMRs originate from
157 abnormal methylation acquisition following successful DNA demethylation in E13.5 PGCs
158 (Figure 1E). Because methylated H3K4 protects the genome from targeting by *de novo* DNMTs,
159 we posit that diminished H3K4me3 in *Tet1*$^{-/-}$ prospermatogonia increases DNMT3A/3L access,
160 leading to aberrant methylation at these regions. Assessing H3K4me3 signals and *Tet1*$^{-/-}$ sperm
161 hypermethylated DMR subsets showed that those originating from abnormal methylation
162 (hypermorphic and ectopic) corresponded to regions with H3K4me3 erosion in
163 prospermatogonia, while those originating from incomplete methylation erasure did not show
164 changes in H3K4me3 signals (Figure 2D). DMRs specific to *Tet1*$^{-/-}$ PGCs also showed no
165 H3K4me3 changes at the prospermatogonia stage, suggesting a decoupling between the role of
166 TET1 in DNA demethylation during reprogramming and its role in patterning the chromatin for
167 *de novo* methylation acquisition (Figure 2D). Incidences of abnormal methylation gain that
168 coincide with H3K4me3 reduction in *Tet1*$^{-/-}$ prospermatogonia can be found in both genic and
169 intergenic regions (Figure 2E). ICRs such as those from *Nespas/Gnas* locus, where
170 hypermethylation originated from incomplete methylation erasure (Supplemental Fig. 1B), had
171 largely unchanged H3K4me3 in *Tet1*$^{-/-}$ prospermatogonia (Figure 2E).
172 H3K4me3 is highly enriched at TSSs of active genes in eukaryotic cells (Barski et al.
173 2007; Schneider et al. 2004). While there is strong evidence that H3K4me3 can serve as a
174 recognition signal for the transcription initiation complex, transcription can still occur without
175 H3K4me3 because the mark may not be instructive for gene expression genome wide (Lauberth
176 et al. 2013; Clouaire et al. 2012). We assessed the relationship between H3K4me3 changes

177 and gene expression in *Tet1*$^{-/-}$ prospermatogonia. While total RNA sequencing revealed many
178 differentially expressed genes in *Tet1*$^{-/-}$ prospermatogonia (DEGs: 2035 upregulated, 4772
179 downregulated; Supplemental Fig. 3A; Supplemental Table S4A), we did not observe any
180 directional correlations to changes in H3K4me3 (Figure 3A, Supplemental Table S4B). Perhaps
181 consistent with the known promiscuity or leakiness of gene expression in the male germline,
182 where up to 80% of all protein-coding genes can be detected at any given developmental stage,
183 DEGs are associated with biological processes at much later stages of spermatogenesis (e.g.
184 downregulation of motility-associated genes and upregulation of chromosome segregation
185 during meiosis-associated genes; Supplemental Fig. 3B, C) (Xia et al. 2020). Overall, our data
186 showed that H3K4me3 in prospermatogonia does not direct global gene expression.
187 To explore the regulatory potential of these altered regions across spermatogenesis, we
188 performed chromatin state discovery using ChromHMM. We built segmentation models from
189 publicly available histone PTMs, Pol2, and CTCF ChIP-seq datasets (Supplemental Fig. 3D,
190 Supplemental Table 5) spanning five stages of spermatogenesis: SSCs, differentiated
191 spermatogonia (SPG), pachytene spermatocyte (PS), round spermatid (RS), and sperm. We
192 assigned chromatin states based on Roadmap Epigenomics Consortium conventions
193 (Supplemental Fig. 3D) (Ernst and Kellis 2012) . Regions that gained H3K4me3 in *Tet1*$^{-/-}$
194 prospermatogonia matched canonical TSS, while regions with depleted H3K4me3
195 corresponded to enhancer-like states (Figure 3B). Regions with reduced H3K4me3 in *Tet1*$^{-/-}$
196 prospermatogonia were enriched for long terminal repeats (LTRs) and LINE elements
197 (Supplemental Fig. 3E). Motif enrichment analysis after repeat masking identified recognition
198 sites for methylation sensitive ETS and HOX families of transcription factors (Figure 3C)
199 (Stephens and Poon 2016; Huang et al. 2012) . Consistent with potentially serving as promoters
200 that are relevant for male germ line development (Supplemental Fig. 3F), regions that gained
201 H3K4me3 in *Tet1*$^{-/-}$ prospermatogonia contain motifs for DMRT6 binding, a germ cell-specific,

202 methylation sensitive transcription factor that coordinates the mitosis to meiosis transition
203 (Figure 3D) (Zhang et al. 2014).
204 Our findings support the hypothesis that non-catalytic domains of TET1 contribute to
205 H3K4me3 deposition, which protect intergenic sperm HMRs from *de novo* methylation
206 acquisition. Indeed, emerging evidence shows that non-catalytic domains of TET1 within the C-
207 terminus interact with chromatin modifiers in development and disease (Lian et al. 2016; Joshi
208 et al. 2022). We previously generated a mouse line with the *Tet1*$^{H1654Y,D1656A(HXD)}$ mutation, which
209 produces a catalytically inactive but full-length TET1 protein (Ko et al. 2011; Chrysanthou et al.
210 2022; Caldwell et al. 2021; Prasasya et al. 2024). To test whether non-catalytic TET1
211 expression is sufficient to establish the chromatin landscape for proper male germline *de novo*
212 methylation, we analyzed *Tet1*$^{HxD/HxD}$ prospermatogonia.
213 We conducted CUT&RUN for H3K4me3 in *Tet1*$^{HxD/HxD}$ prospermatogonia at E17.5. In
214 support of our hypothesis, the majority of H3K4me3 changes seen in *Tet1*$^{-/-}$ prospermatogonia
215 were absent in *Tet1*$^{HxD/HxD}$ compared to WT (Figure 4A, Supplemental Fig. 4A, Supplemental
216 Table S2C). Of the regions that lost H3K4me3 in *Tet1*$^{-/-}$ prospermatogonia, over 89% (20494 of
217 22904) were restored to WT levels in *Tet1*$^{HxD/HxD}$ (Figure 4A, Supplemental Fig. 4A,
218 Supplemental Table S3C, D). The genomic distribution of H3K4me3 consensus peaks in
219 *Tet1*$^{HxD/HxD}$ prospermatogonia was comparable to *Tet1*$^{-/-}$ and WT and consistently overlapped
220 with sperm HMRs (Supplemental Fig. 4B-C). At both TSS-centered and intergenic peaks,
221 H3K4me3 signals in *Tet1*$^{HxD/HxD}$ prospermatogonia showed intermediate levels between WT and
222 in *Tet1*$^{-/-}$ (i.e. increased around TSSs and decreased at intergenic peaks; Supplemental Fig. 4D-
223 E).
224 The limited number of regions where H3K4me3 was depleted in *Tet1*$^{HxD/HxD}$
225 prospermatogonia (compared to WT) remained associated with eventual hypermethylated
226 DMRs in *Tet1*$^{HxD/HxD}$ sperm, although the overlap was significantly reduced compared to *Tet1*$^{-/-}$

227 germ cells (Figure 4B-C). Among 5631 hypermethylated DMRs identified in *Tet1*$^{-/-}$ sperm, 3710
228 (~2/3) were not significantly hypermethylated in *Tet1*$^{HxD/HxD}$ sperm (defined as rescued DMRs)
229 (Prasasya et al. 2024). These methylation defects cannot be fully attributed to loss of TET1
230 catalytic activity. Of note, regions that remained hypermethylated in *Tet1*$^{HxD/HxD}$ sperm are those
231 that require TET1-iterative oxidation capability such as ICRs and promoter of germline
232 responsive genes (Prasasya et al. 2024).

233 We examined how H3K4me3 enrichment in prospermatogonia relates to the rescue of
234 sperm hypermethylation defects in *Tet1*$^{HxD/HxD}$ compared to *Tet1*$^{-/-}$ sperm. To determine whether
235 restoration of H3K4me3 in *Tet1*$^{HxD/HxD}$ prospermatogonia underlies this rescue, we compared
236 H3K4me3 signal intensity across rescued and not-rescued DMRs in *Tet1*$^{HxD/HxD}$ and *Tet1*$^{-/-}$
237 (Figure 4D, Supplemental Table S3E-F). Overall, both DMR subsets exhibited higher H3K4me3
238 levels in *Tet1*$^{HxD/HxD}$ than in *Tet1*$^{-/-}$ prospermatogonia, consistent with a global restoration of this
239 mark in *Tet1*$^{HxD/HxD}$ prospermatogonia (Figure 4A, Supplemental Fig. 4A). To quantify the extent
240 of H3K4me3 restoration toward WT levels, we calculated the fold-change of H3K4me3 signal in
241 *Tet1*$^{HxD/HxD}$ relative to *Tet1*$^{-/-}$ prospermatogonia. The degree of restoration was significantly
242 greater across rescued DMRs than across those that remained hypermethylated (not-rescued;
243 Figure 4E), indicating that a threshold of partial recovery of H3K4me3 in *Tet1*$^{HxD/HxD}$
244 prospermatogonia correlates with absence of hypermethylation in *Tet1*$^{HxD/HxD}$ sperm.

245 To test this relationship more formally, we performed permutation based enrichment
246 analysis to assess whether rescued DMRs preferentially overlapped regions showing restored
247 H3K4me3 in *Tet1*$^{HxD/HxD}$ prospermatogonia (Gel et al. 2015). Both rescued and not-rescued
248 DMRs showed significant enrichment within H3K4me3 restored peaks in *Tet1*$^{HxD/HxD}$
249 prospermatogonia (Supplemental Fig. 4F-G), but the effect size (Z-score) was markedly higher
250 for rescued DMRs (Figure 4F). Together, these results indicate that non-catalytic full length
251 TET1^{HxD} is sufficient to enhance H3K4me3 deposition in prospermatogonia compared to the

252 absence of TET1, yet only regions surpassing a threshold of H3K4me3 enrichment achieve
253 protection from DNMT3A/3L-mediated *de novo* methylation (illustrated in Figure 4G).
254 In the male germline, hypermethylation is required, in part, to silence retroelements that
255 are toxic for meiosis (Bourc'his and Bestor 2004; Barau et al. 2016). Despite this, certain
256 regions of the mammalian sperm genome resist DNA methylation, including CpG-dense
257 promoters and younger, species-specific transposon subfamilies overlapping regulatory
258 elements (Shirane and Lorincz 2023; Molaro et al. 2011). Additionally, low methylation at CpG-
259 dense regions correlates with nucleosome retention during histone-to-protamine exchange, a
260 critical step male gamete maturation (Erkek et al. 2013) . Retained nucleosomes in sperm play
261 a crucial role in patterning chromatin of the early embryo, underscoring the importance of the
262 sperm epigenome beyond spermatogenesis (Fanourgakis et al. 2025). Thus, the integrity of
263 sperm HMRs is essential for both spermatogenesis and potentially embryo viability.
264 We previously demonstrated that most methylation defects from compromised TET1
265 activity occur within sperm HMRs (Prasasya et al. 2024). Iterative oxidation is required at ICRs
266 and meiosis-associated promoters, but these account for only a small fraction of *Tet1*$^{-/-}$ sperm
267 defects. In addition to its role in active demethylation, TET1 has been proposed protect against
268 DNA re-methylation during epigenetic reprogramming (Hill et al. 2018). However, DNMT3A/3L
269 activity is limited at E14.5, making this role less likely in PGCs. Our findings instead suggest a
270 role for TET1 in preventing abnormal methylation acquisition in prospermatogonia. Aberrant
271 DNA methylation in *Tet1*$^{-/-}$ sperm coincides with erosion of H3K4me3 in prospermatogonia, the
272 chromatin feature that protects and patterns sperm HMRs (Figure 4G). Consistently, the non-
273 catalytic function of TET1, as tested in *Tet1*$^{HxD/HxD}$ germline, is sufficient enhance H3K4me3
274 deposition and partially rescue DNA methylation (Prasasya et al. 2024). Analysis of H3K4me3
275 enrichment in *Tet1*$^{HxD/HxD}$ prospermatogonia suggests that there is likely a threshold of H3K4me3
276 that is needed to protect sperm HMRs from the activity of DNMT3A/3L during *de novo*

277 methylation as not all regions with H3K4me3 restoration corresponds to rescue of DNA
278 hypermethylation (Figure 4G).
279 TET proteins interact with chromatin modifiers in many contexts. In embryonic stem cells
280 (ESCs), the non-catalytic function of TET1 shapes bivalency (H3K4me3, H3K27me3) at
281 regulators of mesoderm and trophectoderm lineages by recruiting Polycomb repressive complex
282 2 (PRC2) and Sin3a (Chrysanthou et al. 2022) . TET1 is also a stable binding partner of *O*-
283 GlcNAc transferase (OGT) and is required for OGT-Sin3a-Hcf1 binding to chromatin (Vella et al.
284 2013; Williams et al. 2011). Hcf1 is a key component of the SET1/COMPASS histone
285 methyltransferase complex, a writer for H3K4me2/3. In hematopoiesis, the TET2/3-OGT
286 complex promotes Hcf1 O-GlcNAcylation, leading to SET1/COMPASS assembly, H3K4me3
287 deposition, and gene activation (Capotosti et al. 2011; Deplus et al. 2013). A similar mechanism
288 may apply in prospermatogonia, as single cell RNA-seq confirms *Ogt* and *Hcfc1* expression in
289 fetal and neonatal germ cells, coinciding with *de novo* methylation (Zhao et al. 2021).
290 It is also possible that in addition to promoting H3K4me3 deposition, TET1 may also
291 partially restrain DNA methylation by physically protecting its targets from DNMT3A/3L in
292 prospermatogonia. This is not likely to be the main mechanism of sperm HMRs protection
293 however, as TET1 and DNMT3A antagonism was previously found to be highly context
294 dependent within proximal promoters (Gu et al. 2018). Furthermore, in human ESCs, TET1 and
295 DNMT3A have been shown to co-bind, especially within DNMT3A preference binding regions
296 (Chao et al. 2022). Notably, TET1-dependent sperm HMRs are intergenic and acquire
297 enhancer-like chromatin states throughout spermatogenesis (Figure 2A, 3B). Top enriched
298 motifs in these regions correspond to ETS transcription factors. Significantly, the ETS family of
299 transcription factors are known to interact with and recruit histone acetyltransferases such as
300 CBP and p300, in further support of the potential of intergenic sperm HMRs as regulatory
301 elements (Yang et al. 1998; Goodman and Smolik 2000). We propose that protecting intergenic
302 sperm HMRs from methylation helps establish the enhancer landscape that regulates stage-

303 specific gene expression, particularly during the mitosis-to-meiosis transition (Maezawa et al.
304 2020). Indeed, *Tet1*$^{-/-}$ male mice reproductive defects are attributed to premature aging due to
305 reduced SSCs and progressively worse meiotic defects (Huang et al. 2020). While the
306 mechanism orchestrating chromatin patterning before *de novo* methylation remains unclear, our
307 findings reveal the non-catalytic function of TET1 as a key determinant in establishing sperm
308 HMRs.
309

310 **Methods**

311 *Mouse models and germ cell collection*

312 All experiments were approved by the Institutional Animal Care and Use Committee of the
313 University of Pennsylvania (protocol number: 804211). Mice were housed in polysulfone cages
314 within a pathogen-free facility under a 12 h light/dark cycle, with ad libitum access to water and
315 standard chow (Laboratory Autoclavable Rodent Diet 5010, LabDiet, St. Louis, MO, USA). *Tet1*
316 knockout mice (Dawlaty et al. 2013) (017358; B6;129S4-Tet1$^{tm1.1Jae}$/J) and *Oct4-GFP* mice
317 (Lengner et al. 2007) (008214; B6;129S4-Pou5f1^{tm2Jae}/J) were obtained from The Jackson
318 Laboratory and backcrossed for at least 10 generations to a C57BL/6J background (000664;
319 B6; The Jackson Laboratory). Catalytically inactive *Tet1*^{HxD} mouse line was generated as
320 described in (Prasasya et al. 2024). The *Oct4-GFP* allele was maintained as homozygous in
321 *Tet1* heterozygote breeders (*Tet1*$^{+/-}$; *Oct4*$^{GFP/GFP}$ or *Tet1*$^{HxD/+}$; *Oct4*$^{GFP/GFP}$). Primers to determine
322 sex, *Tet1*$^{tm1.1Jae}$, *Tet1*^{HxD}, and *Oct4-GFP* alleles are listed in Supplemental Table S6.

323 Gonadal tissues from E13.5 and E17.5 embryos (post copulatory plug detection) were dissected
324 and digested into a single-cell suspension using 0.25% trypsin/EDTA for 10 minutes at 37 °C.
325 *GFP*$^{+}$ germ cells were isolated by flow cytometry. For bisulfite mutagenesis and RNA isolation,
326 germ cells were sorted into empty tubes and immediately snap-frozen for storage at -80 °C until
327 processing. For CUT&RUN, sorted cells were collected into chilled PGC medium (DMEM
328 supplemented with 15% FBS, 100 U/mL leukemia inhibitory factor, 5 μM forskolin, 1 ng/mL stem
329 cell factor). Following sorting, dimethyl sulfoxide (DMSO) was added to a final concentration of
330 10%, and the cells were slow frozen using Mr. Frosty until library preparation.

331 *Genome-wide DNA methylation profiling using Infinium Mouse Methylation BeadChip*

332 Snap frozen germ cell pellet was directly lysed and bisulfite mutagenized using EZ DNA
333 Methylation Direct Kit (Zymo Research) per manufacturer's instructions. Bisulfite mutagenized
334 (BSM) DNA was subjected to low-input whole-genome amplification workflow prior to
335 hybridization to Illumina BeadChip array as detailed in (Lee et al. 2024) (Workflow J). Briefly,
336 BSM DNA underwent 2 rounds of Klenow amplifications (NEB) using random hexamer primers
337 (NEB). For additional details on library preparation and data analysis, see the Supplemental
338 Material. Amplified DNA was cleaned using solid-phase reversible immobilization (SPRI) beads

339 (2x; Beckman Coulter) and concentration was measured with Qubit (Invitrogen).10 µL of BSM
340 DNA library was submitted for hybridization onto the Infinium Mouse Methylation-12v1-0
341 BeadChip (Illumina) at Children's Hospital of Philadelphia Center for Applied Genomics.

342 *CUT&RUN library preparation*

343 CUT&RUN experiments were performed on samples of 4,000 nuclei isolated per epitope from
344 cryopreserved germ cells as described above using CUTANA ChIC/CUT&RUN kit (EpiCypher).
345 Three biological replicates per genotype were prepared for H3K4me3 (1:100, Cell Signaling
346 Technology antibody 2729) and IgG (1:50, CUTANA Rabbit IgG negative control antibody). Cells
347 were rapidly thawed and counted, followed by nuclei extraction using NE buffer (20 mM
348 HEPES-KOH pH 7.9, 10mM KCl, 0.5 mM fresh spermidine, 0.1% Triton X-100, 20% glycerol
349 plus protease inhibitors). Nuclei were bound to concanavalin A-coated magnetic beads and
350 CUT&RUN was conducted per CUTANA product manual with modifications. CUT&RUN libraries
351 were prepared with NEBNext Ultra II DNA Library Prep Kit for Illumina (NEB). For additional
352 details on library preparation and data analysis, see the Supplemental Material.

353 *Total RNAseq library preparation*

354 Total RNA was extracted from 5000 snap frozen E17.5 germ cells isolated from a single embryo
355 using TRIzol reagent (Invitrogen). RNA integrity number and concentration were assessed using
356 the High Sensitivity RNA ScreenTape for TapeStation system (Agilent Technologies). Ribosomal
357 RNA-depleted total RNA libraries were generated using the SMART-Seq Total RNA Pico Input
358 Kit with UMIs with ZapR Mammalian (Takara Bio) from 5 ng input according to the
359 manufacturer's protocol. Libraries were indexed with NEBNext Multiplex Oligos for Illumina
360 Unique Dual Index Primer Pairs (NEB) and were amplified using SeqAmp DNA Polymerase
361 (Takara Bio). For additional details on library preparation and data analysis, see the
362 Supplemental Material.

363 *Data availability*

364 Data will be submitted to NIH Gene Expression Omnibus once US government resumes
365 operation. Raw, analyzed, and corresponding meta data are currently hosted on Box and
366 access will be granted upon request for review purposes.

367 **Acknowledgement**

368 This work was supported by National Institute of Health grant numbers R01GM146388 (MSB),

369 R01GM051279 (MSB), R01GM118501 (RMK), R01HG010646 (RMK), K99HD112543 (RDP).

370 *Authors contribution*

371 Experiments were designed by RDP with assistance and supervision from MSB and RMK. JJK

372 and RDP collected samples and performed all experiments. ZL performed initial quality check

373 and alignment for CUT&RUN and RNAseq experiments. Data and statistical analysis for

374 methylation array, CUT&RUN and RNAseq was performed by RDP. JJK illustrated the summary

375 figure. RDP wrote the manuscript, which was approved by all authors.

Figures and figure legends

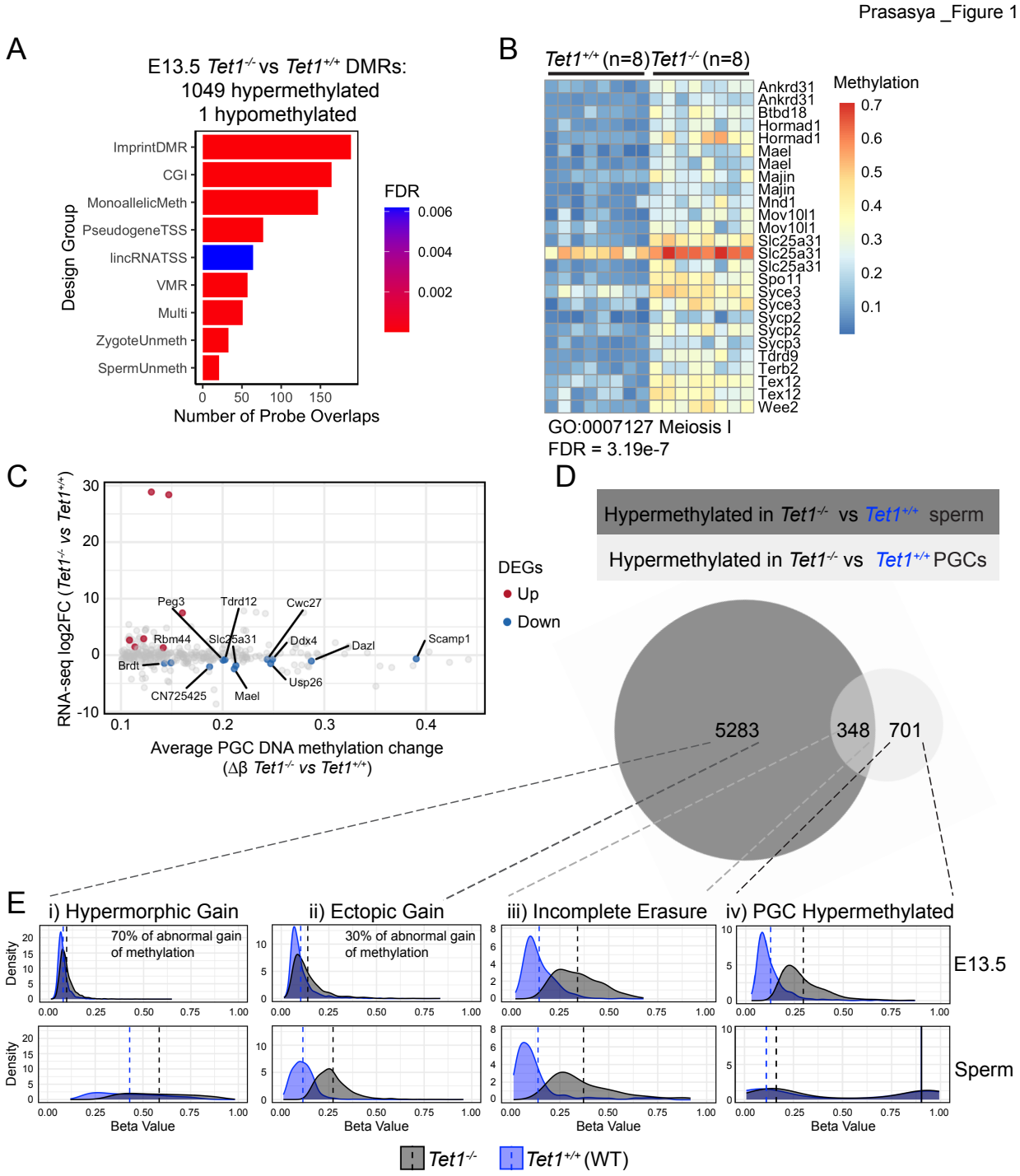

379 **Figure 1. The majority of methylation defects in *Tet1*$^{-/-}$ sperm do not result from**

380 **incomplete methylation erasure during epigenetic reprogramming.**

381 A) Top enriched design groups based on the Illumina Infinium Mouse Methylation BeadChip

382 manifest for hypermethylated DMRs in *Tet1*$^{-/-}$ PGCs.

383 B) Heatmap of probes associated with the most enriched GO term among hypermethylated

384 DMRs in *Tet1*$^{-/-}$ PGCs.

385 C) Scatterplot showing overlap between hypermethylated DMRs and DEGs in *Tet1*$^{-/-}$ PGCs.

386 D) Comparison of hypermethylated probes (differentially methylated regions, DMRs: FDR ≤

387 0.05; >10% methylation difference) in E13.5 *Tet1*$^{-/-}$ PGCs (n=8) vs *Tet1*$^{+/+}$ (WT, n=8) and those

388 previously reported in *Tet1*$^{-/-}$ sperm (Prasasya et al. 2024).

389 E) Methylation levels in E13.5 PGCs (top) or sperm (bottom) for *Tet1*$^{-/-}$ (black) and *Tet1*$^{+/+}$ (blue).

390 DMRs are subsetted by origin of hypermethylation (i–iv). Average methylation levels are

391 denoted by dotted vertical lines.

392

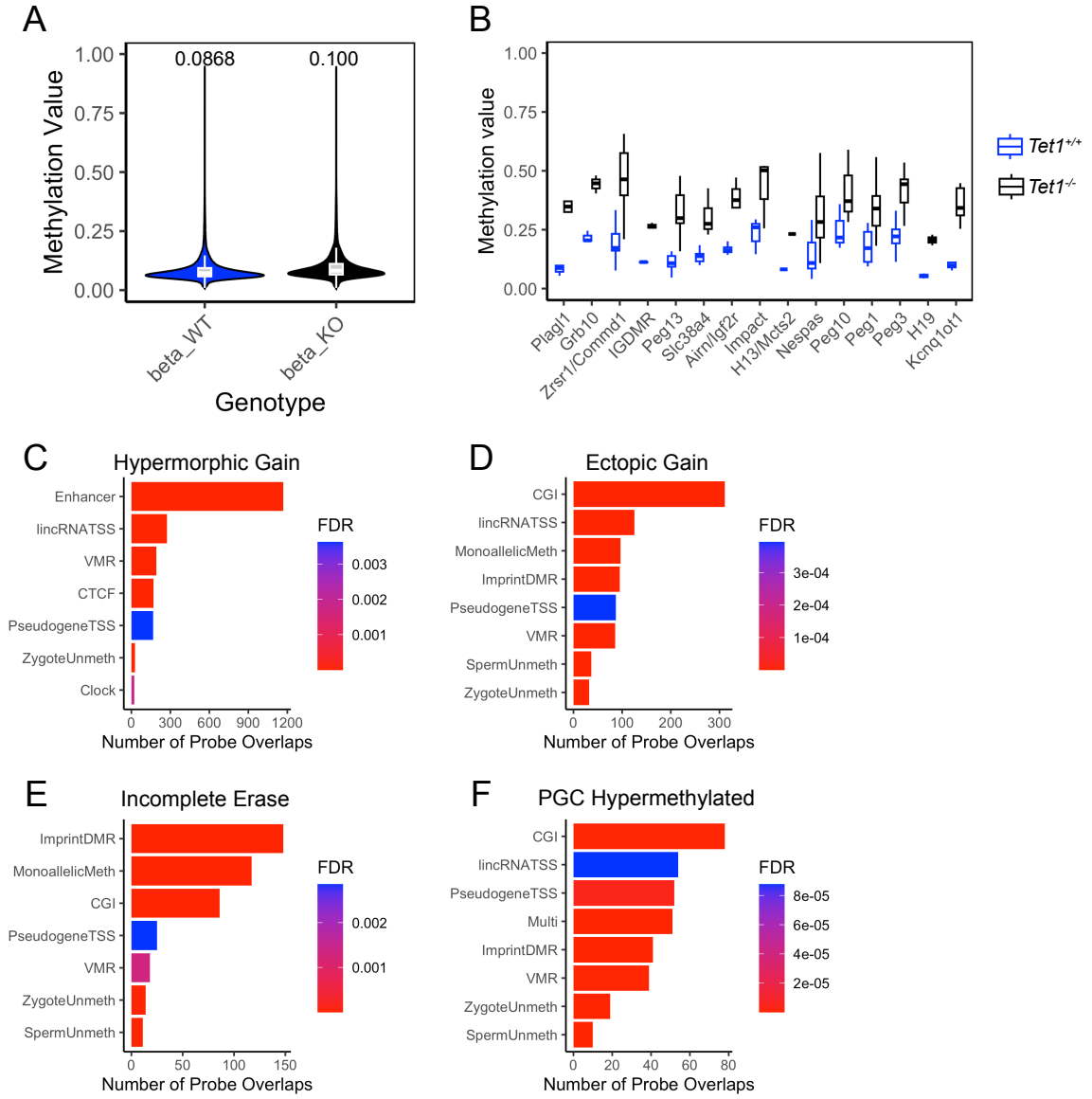
A
Methylation Value
1.00
0.75
0.50
0.25
0.00
0.0868
0.100
beta_WT
beta_KO
Genotype
B
Methylation value
1.00
0.75
0.50
0.25
0.00
Plagl1
Grb10
Zrsr1/Commd1
IGDMR
Peg13
Slc38a4
Airn/Igf2r
Impact
H13/Mcts2
Nespas
Peg10
Peg1
Peg3
H19
Kcnq1ot1
Tet1+/+
Tet1-/-
C
Hypermorphic Gain
Enhancer
lincRNATSS
VMR
CTCF
PseudogeneTSS
ZygoteUnmeth
Clock
FDR
0.003
0.002
0.001
0
300
600
900
1200
Number of Probe Overlaps
D
Ectopic Gain
CGI
lincRNATSS
MonoallelicMeth
ImprintDMR
PseudogeneTSS
VMR
SpermUnmeth
ZygoteUnmeth
FDR
3e-04
2e-04
1e-04
0
100
200
300
Number of Probe Overlaps
E
Incomplete Erase
ImprintDMR
MonoallelicMeth
CGI
PseudogeneTSS
VMR
ZygoteUnmeth
SpermUnmeth
FDR
0.002
0.001
0
50
100
150
Number of Probe Overlaps
F
PGC Hypermethylated
CGI
lincRNATSS
PseudogeneTSS
Multi
ImprintDMR
VMR
ZygoteUnmeth
SpermUnmeth
FDR
8e-05
6e-05
4e-05
2e-05
0
20
40
60
80
Number of Probe Overlaps

393

394

395 **Supplemental Figure 1. Additional analysis of methylation arrays for Tet1-/- vs Tet1+/+**
396 **PGCs.**

397 A) Violin plots of average methylation values at each CpG probe with overall mean methylation
398 indicated (n=8 per group). Differentially methylated probes were identified using limma (FDR ≤
399 0.05, >10% difference).

400 B) ICRs are the most enriched design-group category among hypermethylated DMRs in *Tet1*$^{-/-}$
401 PGCs (15 of 21 array-represented ICRs are significantly hypermethylated). Boxplots show
402 average methylation of probes associated with hypermethylated ICRs.

403 C–F) Top enriched Infinium Mouse Methylation BeadChip design groups for different categories
404 of *Tet1*$^{-/-}$ sperm and PGC DMRs.

405

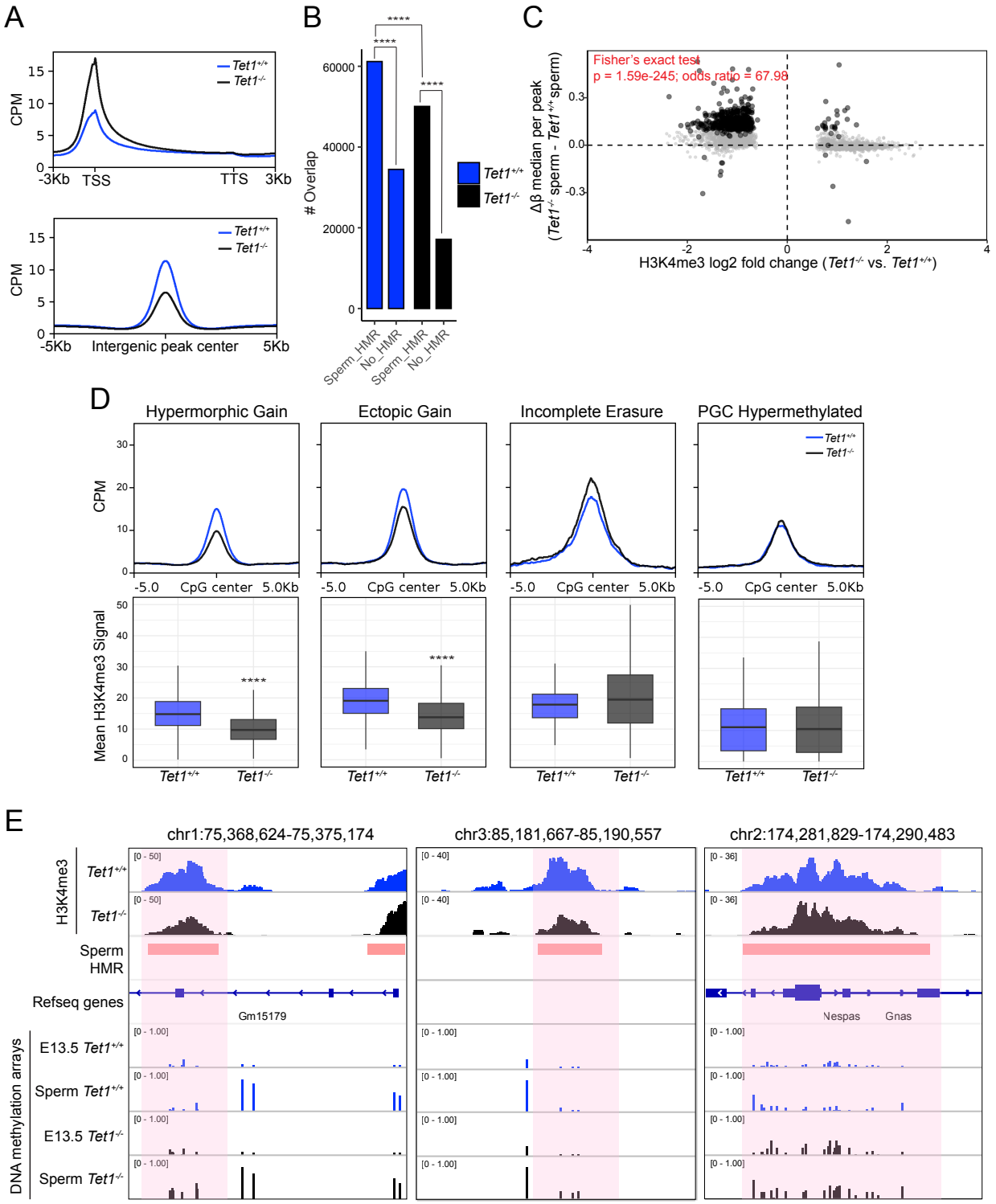
A
CPM
Tet1+/+
Tet1-/-
-3Kb TSS TTS 3Kb
-5Kb Intergenic peak center 5Kb
B
Overlap
Sperm_HMR
No_HMR
C
Fisher's exact test
p = 1.59e-245; odds ratio = 67.98
Δβ median per peak (Tet1-/- sperm - Tet1+/+ sperm)
H3K4me3 log2 fold change (Tet1-/- vs. Tet1+/+)
D
Hypermorphic Gain
Ectopic Gain
Incomplete Erasure
PGC Hypermethylated
-5.0 CpG center 5.0Kb
Mean H3K4me3 Signal
E
chr1:75,368,624-75,375,174
chr3:85,181,667-85,190,557
chr2:174,281,829-174,290,483
H3K4me3
Sperm HMR
Refseq genes
Gm15179
Nespas
Gnas
DNA methylation arrays
E13.5 Tet1+/+
Sperm Tet1+/+
E13.5 Tet1-/-
Sperm Tet1-/-

406

407

408 **Figure 2. Abnormal de novo methylation acquisition is associated with H3K4me3 erosion**
409 **in *Tet1*$^{-/-}$ male germ cells.**
410 A) Metaplot of H3K4me3 signals over genic regions (top) or consensus intergenic peaks
411 (bottom).
412 B) Distribution of H3K4me3 peaks overlapping sperm HMRs compared to non-HMRs (**** $p <$
413 0.0001, Fisher's exact test).
414 C) Scatterplot of *Tet1*$^{-/-}$ sperm DMRs and regions with differential H3K4me3 in *Tet1*$^{-/-}$
415 prospermatogonia. H3K4me3 peaks overlapping with DMRs in *Tet1*$^{-/-}$ sperm are highlighted in
416 black circles. Fisher's exact test for hypermethylated DMRs overlapping H3K4me3-depleted vs
417 other regions.
418 D) (Top) Metagene plots of H3K4me3 signals in *Tet1*$^{-/-}$ and *Tet1*$^{+/+}$ prospermatogonia
419 overlapping subsets of *Tet1*$^{-/-}$ sperm hypermethylated DMRs (hypermorphic gain, ectopic gain,
420 incomplete erasure) or *Tet1*$^{-/-}$ PGC hypermethylated DMRs. (Bottom) Boxplots of mean
421 H3K4me3 signals over 1 kb windows centered on subsets of hypermethylated DMRs (**** $p <$
422 0.0001, Wilcoxon signed-rank test).
423 E) Genome browser tracks for representative sperm hypermethylated DMRs from abnormal de
424 novo methylation at genic region (left) or intergenic region (middle). *Nespas* is a representative
425 ICR that is hypermethylated due to incomplete erasure (right).
426
427
428
429
430

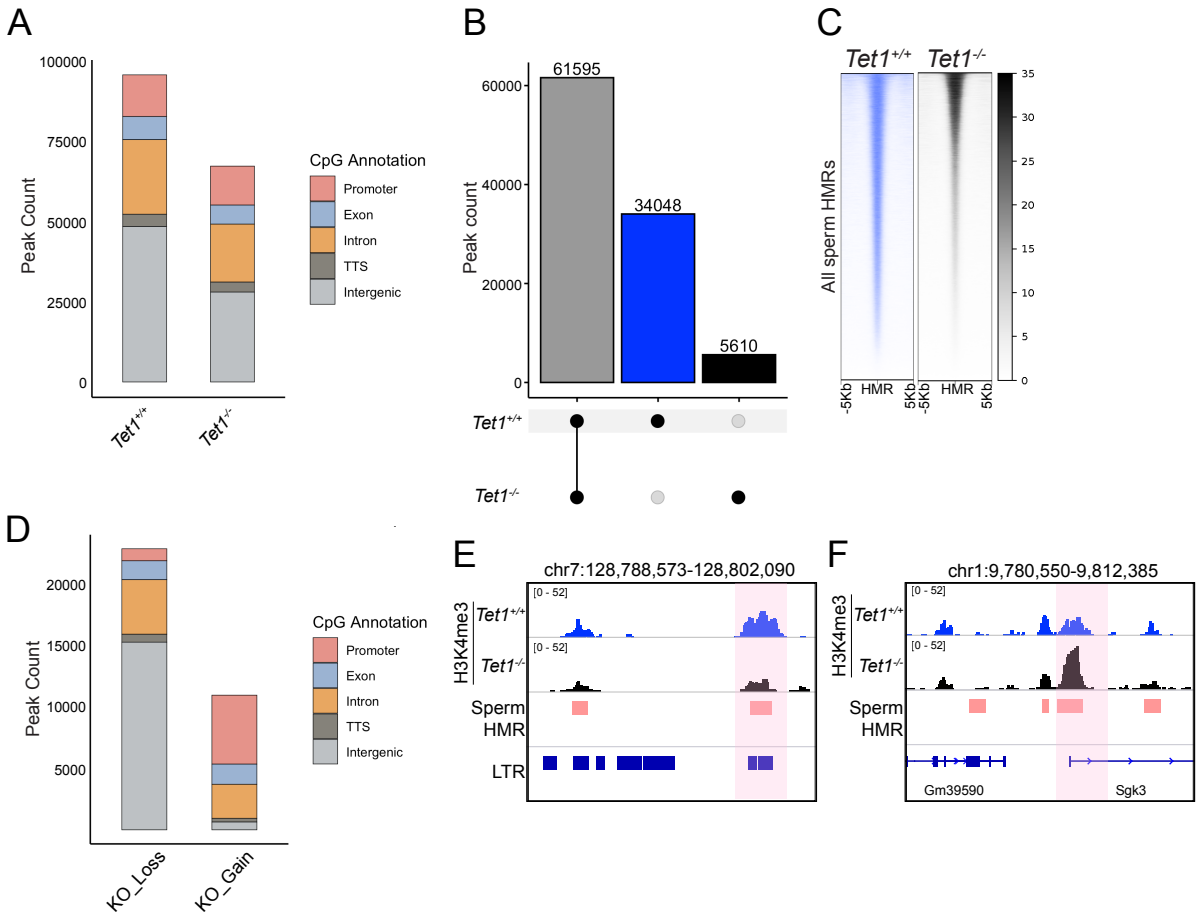
A
Peak Count
100000
75000
50000
25000
0
Tet1+/+
Tet1-/-
CpG Annotation
Promoter
Exon
Intron
TTS
Intergenic
B
Peak count
60000
40000
20000
0
61595
34048
5610
Tet1+/+
Tet1-/-
C
Tet1+/+
Tet1-/-
All sperm HMRs
-5Kb
HMR
5Kb
35
30
25
20
15
10
5
0
D
Peak Count
20000
15000
10000
5000
KO_Loss
KO_Gain
CpG Annotation
Promoter
Exon
Intron
TTS
Intergenic
E
chr7:128,788,573-128,802,090
H3K4me3
Tet1+/+
Tet1-/-
[0 - 52]
Sperm HMR
LTR
F
chr1:9,780,550-9,812,385
H3K4me3
Tet1+/+
Tet1-/-
[0 - 52]
Sperm HMR
Gm39590
Sgk3

431

432

433 **Supplemental Figure 2. Additional analysis of differentially enriched H3K4me3 signals in**

434 ***Tet1*$^{-/-}$ vs *Tet1*$^{+/+}$ prospermatogonia.**

435 A) Genomic compartmentalization of H3K4me3 consensus peaks (present in ≥2 of 3 replicates)

436 in *Tet1*$^{+/+}$ and *Tet1*$^{-/-}$ prospermatogonia.

437 B)) Distribution of H3K4me3 consensus peaks unique to or shared between *Tet1*$^{+/+}$ (n=3) and

438 *Tet1*$^{-/-}$ (n=3) E17.5 prospermatogonia detected by CUT&RUN.

439 C) Heatmaps of H3K4me3 signals in E17.5 *Tet1*$^{-/-}$ and *Tet1*$^{+/+}$ prospermatogonia overlapping

440 sperm hypomethylated regions (HMRs) defined by sperm WGBS (GSE56697; Wang et al.

441 2014). Plots represent averages of 3 biological replicates.

442 D) Genomic distribution of differentially enriched H3K4me3 peaks between *Tet1*$^{-/-}$ and *Tet1*$^{+/+}$

443 prospermatogonia (DiffBind, FDR ≤ 0.05, ≥1.5-fold change).

444 E-F) Genome browser tracks for representative regions showing H3K4me3 loss (E, intergenic)

445 or gain (F, promoter) in *Tet1*$^{-/-}$ prospermatogonia.

446

447

448

449

450

Prasasya_Figure 3

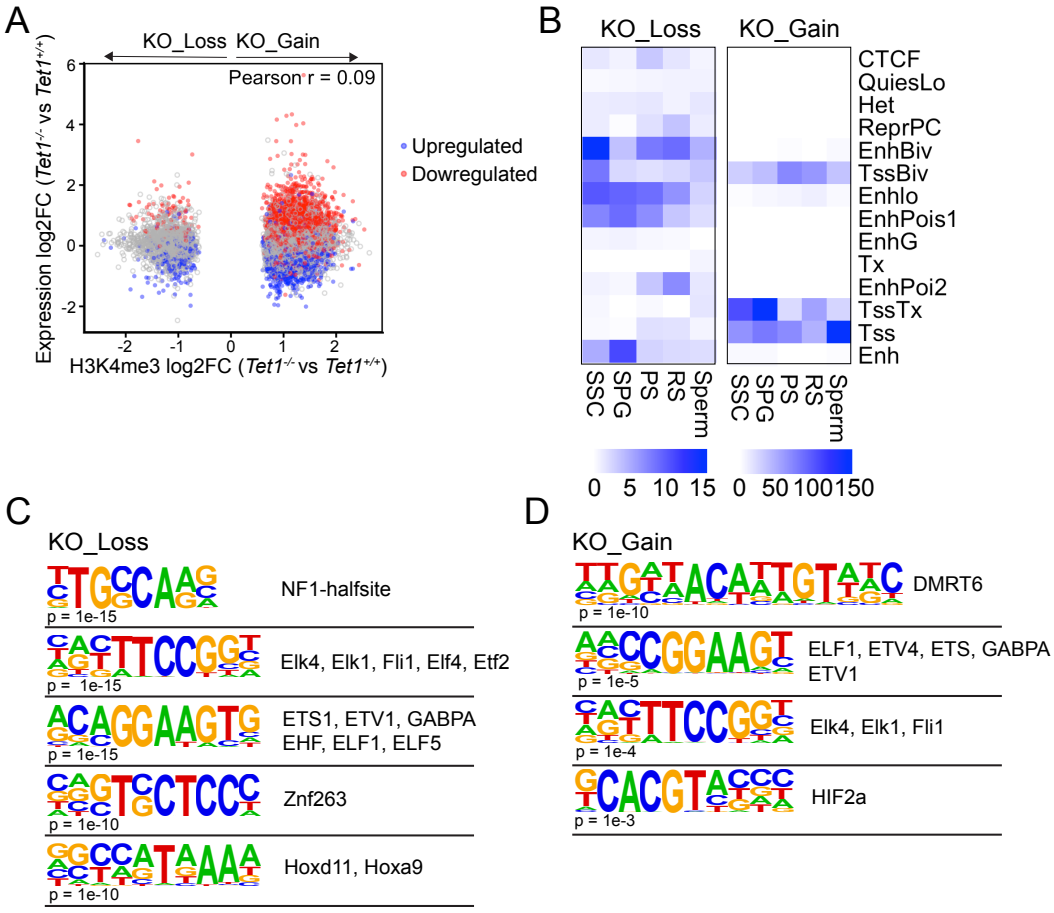

451

452

453 **Figure 3. H3K4me3 enrichment in prospermatogonia may regulate later stages of**
454 **spermatogenesis**
455 A) Scatter plot of significantly altered H3K4me3 peaks in *Tet1*$^{-/-}$ prospermatogonia (vs WT) at
456 gene promoters and their associated gene expression changes as measured by total RNA-seq.
457 Differentially expressed genes (FDR ≤ 0.05, ≥2-fold change) are highlighted with blue
458 (downregulated) or red (upregulated) dots.
459 B) Enrichment of H3K4me3 peaks lost or gained in *Tet1*$^{-/-}$ prospermatogonia across chromatin
460 states during spermatogenesis (SSC: spermatogonial stem cells; SPG: spermatogonia; PS:
461 pachytene spermatocyte; RS: round spermatid), using ChromHMM. Chromatin states
462 assignment is based on the ENCODE consortium projects and are defined in Supplemental Fig.
463 3D (Ernst and Kellis 2017)
464 C) Motif enrichment for regions with H3K4me3 loss after masking repetitive elements.
465 D) Motif enrichment for regions with H3K4me3 gain.
466
467
468
469

Prasasya_Supplemental Fig 3

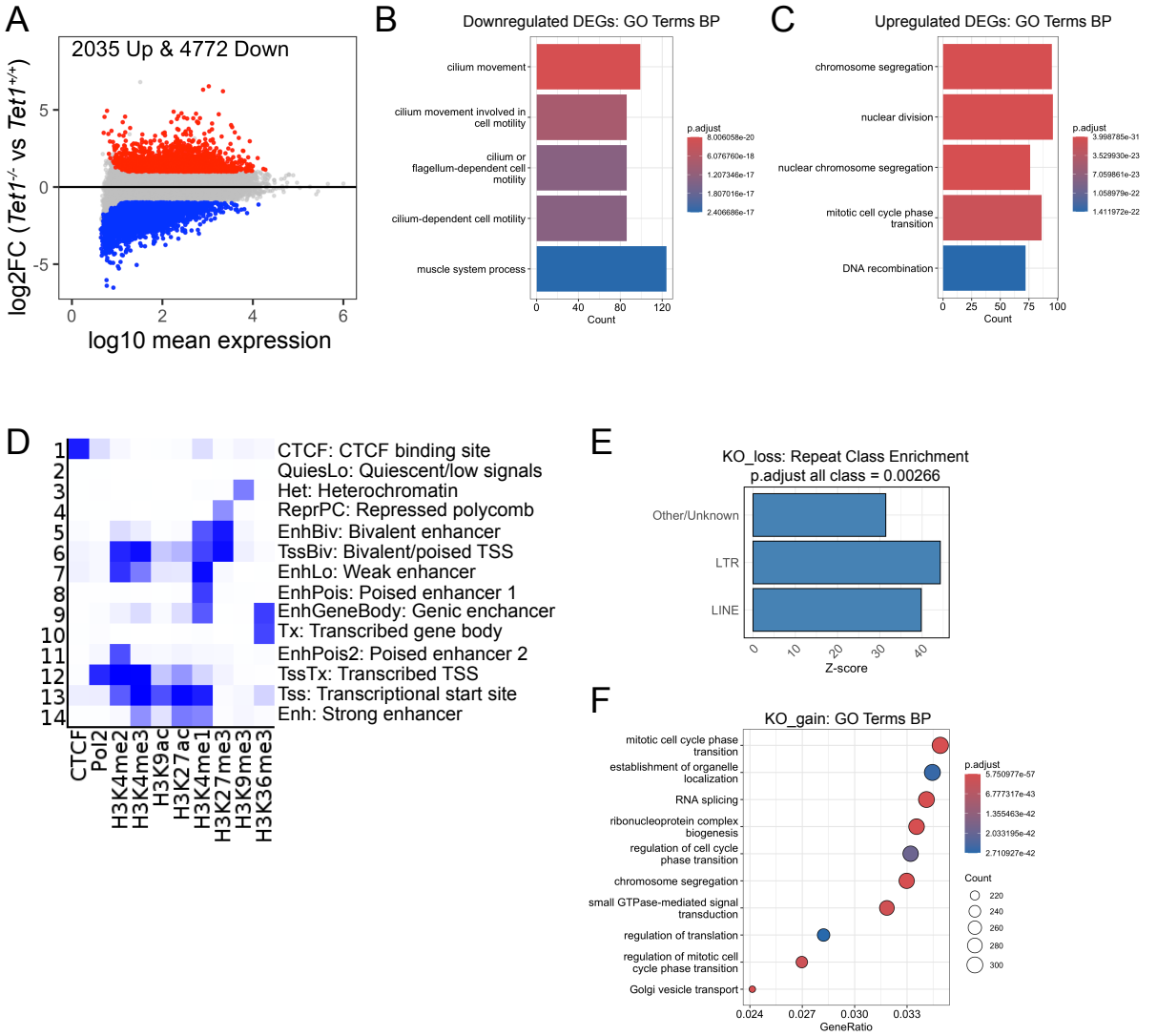

472 **Supplemental Figure 3. Investigation into the potential role of H3K4me3 changes in *Tet1*$^{-/-}$**
473 **prospermatogonia**

474 A) MA-plot for differential expression analysis of total RNA-seq in *Tet1*$^{-/-}$ prospermatogonia vs
475 WT (n=3, FDR ≤ 0.05, ≥2-fold change).

476 B) Top five enriched GO biological process terms for downregulated DEGs in *Tet1*$^{-/-}$
477 prospermatogonia.

478 C) Top five enriched GO biological process terms for upregulated DEGs in *Tet1*$^{-/-}$
479 prospermatogonia.

480 D) Chromatin states assigned by ChromHMM using public datasets for CTCF, Pol II, and
481 histone modifications across spermatogonial stem cells (SSC), spermatogonia (SPG),
482 pachytene spermatocytes (PS), round spermatids (RS), and sperm (datasets used are in
483 supplemental table). Chromatin state assignment is based on Encode consortium convention
484 (Ernst and Kellis 2017).

485 E) Classes of repetitive elements enriched in regions with H3K4me3 loss.

486 F) Top ten enriched GO biological process terms for regions with H3K4me3 gain.

487

Prasasya_Figure 4

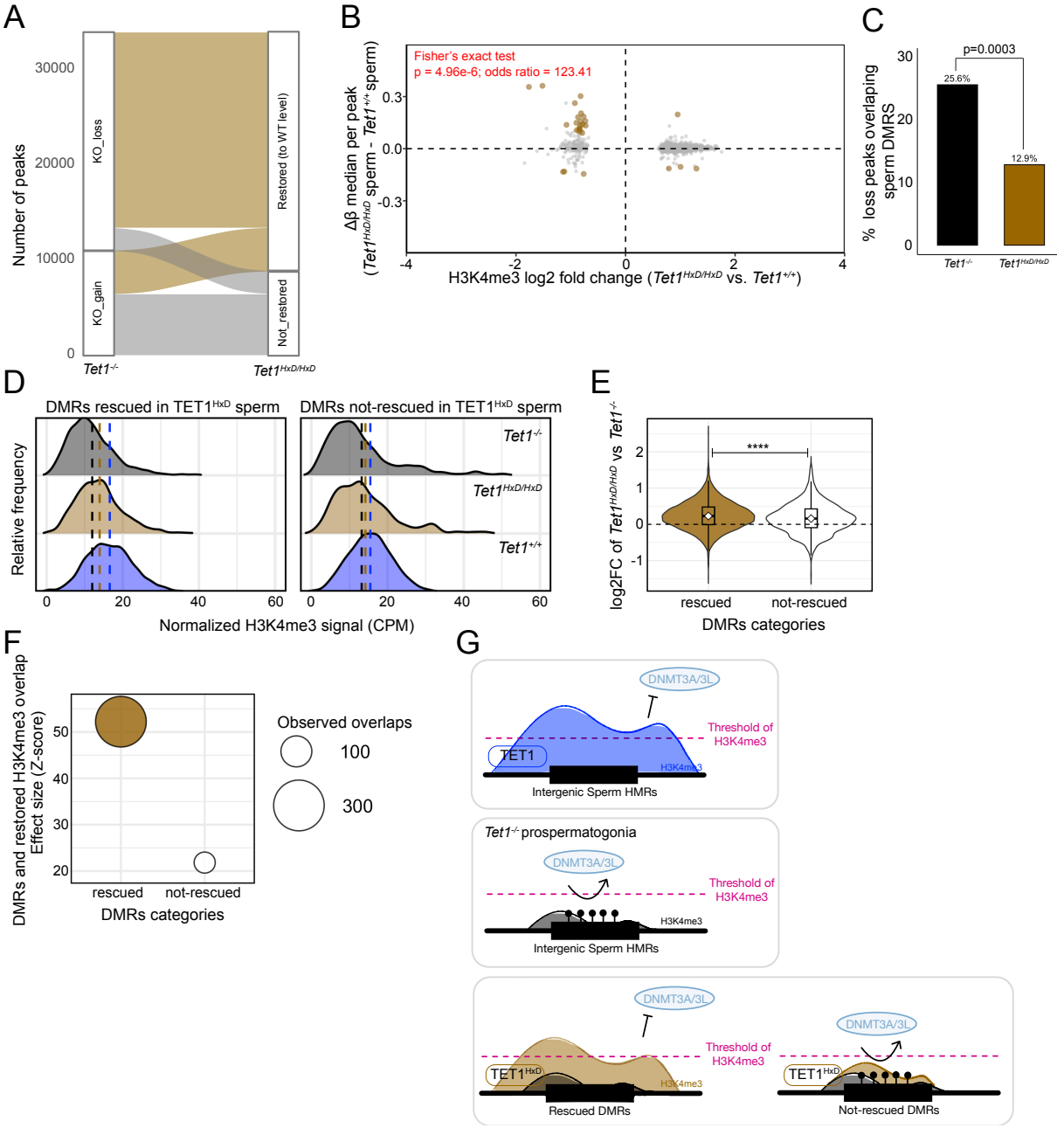

488

489

490 **Figure 4. The non-catalytic, full length TET1^{HxD} restores most H3K4me3 changes in *Tet1*$^{-/-}$**
491 **prospermatogonia.**
492 A) Alluvial plot of differentially enriched H3K4me3 peaks in *Tet1*$^{-/-}$ vs *Tet1*$^{+/+}$ and their status in
493 *Tet1*$^{HxD/HxD}$ vs *Tet1*$^{+/+}$. Light brown ribbons indicate peaks altered in *Tet1*$^{-/-}$ but not in *Tet1*$^{HxD/HxD}$.
494 B) Scatterplot of *Tet1*$^{HxD/HxD}$ sperm DMRs and regions with differential H3K4me3 in *Tet1*$^{HxD/HxD}$
495 prospermatogonia. H3K4me3 peaks overlapping with DMRs in *Tet1*$^{HxD/HxD}$ sperm are highlighted
496 in brown circles. Fisher's exact test for hypermethylated DMRs overlapping H3K4me3-depleted
497 vs other regions.
498 C) Proportion of regions with H3K4me3 loss in Tet1 mutants that overlap hypermethylated
499 sperm DMRs; two-sample proportion test.
500 D) Ridgeline plots showing the relative frequency distribution of DMRs that were significantly
501 hypermethylated in *Tet1*$^{-/-}$ sperm but were not hypermethylated in *Tet1*$^{HxD/HxD}$ sperm (left,
502 rescued DMRs) or stayed hypermethylated in *Tet1*$^{HxD/HxD}$ sperm (right, not-rescued DMRs) and
503 the associated H3K4me3 signals found in *Tet1*$^{+/+}$, *Tet1*$^{-/-}$, or *Tet1*$^{HxD/HxD}$ prospermatogonia. The
504 mean H3K4me3 signal for each genotype across the two subsets of sperm DMRs is indicated
505 with vertical dashed lines of matched colors (blue: *Tet1*$^{+/+}$, black: *Tet1*$^{-/-}$, or brown: *Tet1*$^{HxD/HxD}$)
506 E) Fold change of H3K4me3 signals in *Tet1*$^{HxD/HxD}$ compared to *Tet1*$^{-/-}$ calculated across two
507 subsets of sperm DMRs defined in D (**** $p < 0.0001$, Wilcoxon signed-rank test).
508 F) The strength of overlap between distinct subsets of DMRs (rescued in *Tet1*$^{HxD/HxD}$ sperm or
509 not-rescued in *Tet1*$^{HxD/HxD}$ sperm) and regions where H3K4me3 was restored to WT levels in
510 *Tet1*$^{HxD/HxD}$ prospermatogonia following observed depletion in *Tet1*$^{-/-}$ prospermatogonia as
511 determined by permutation test (Z-score from 1000 permutations of randomly selected regions
512 consistent with Illumina Bead Chip array coverage).
513 G) With the absence of TET1, depletion of H3K4me3 at sperm HMRs (largely located at
514 intergenic regions) is associated with aberrant methylation acquisition in prospermatogonia (top
515 and middle panels). In the presence of full-length TET1^{HxD}, H3K4me3 deposition in

516 spermatogonia is globally increased but only a subset of intergenic sperm HMRs escaped

517 abnormal methylation acquisition in *Tet1*$^{HxD/HxD}$ sperm (bottom panel). Shaded regions indicate

518 relative H3K4me3 signals for each genotype, closed lollipops depict methylated CpGs.

519

Prasasya_Supplemental Fig 4

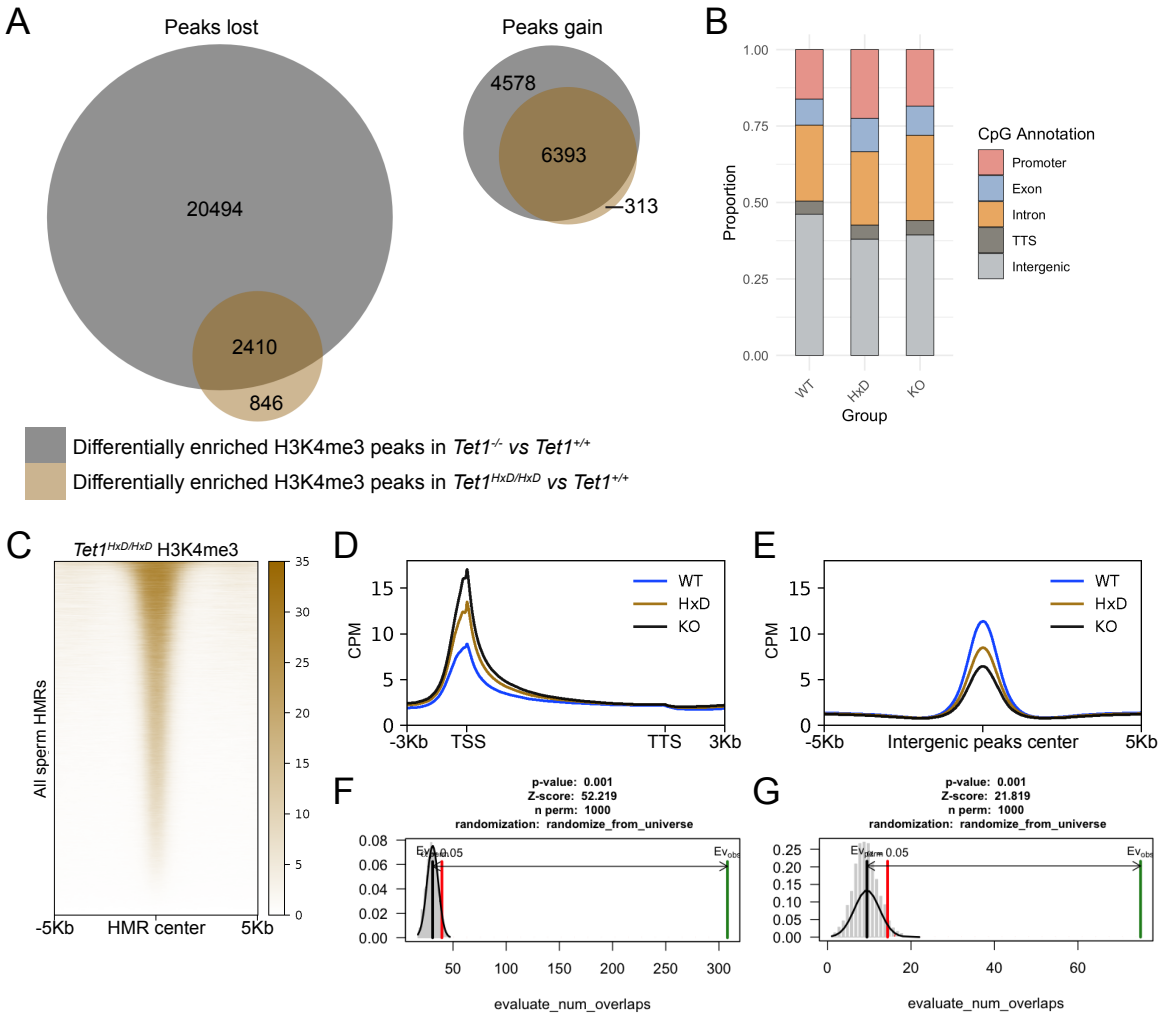

523 **Supplemental Figure 4. Extended CUT&RUN analysis for H3K4me3 in *Tet1*$^{HxD/HxD}$**
524 **prospermatogonia.**

525 A) Venn diagrams of differentially enriched peaks in *Tet1*$^{-/-}$ vs *Tet1*$^{+/+}$ and *Tet1*$^{HxD/HxD}$ vs *Tet1*$^{+/+}$
526 prospermatogonia (DiffBind, FDR ≤ 0.05, ≥1.5-fold change).

527 B) Genomic compartmentalization of consensus peaks (≥2 of 3 replicates) in *Tet1*$^{+/+}$, *Tet1*$^{HxD/HxD}$,
528 and *Tet1*$^{-/-}$ prospermatogonia.

529 C) Heatmaps of H3K4me3 signals in E17.5 *Tet1*$^{HxD/HxD}$ prospermatogonia overlapping sperm
530 HMRs defined by WGBS (GSE56697; Wang et al. 2014). Plots represent averages of 3
531 replicates.

532 D–E) Metaplots of H3K4me3 signals over genic regions (D) or intergenic consensus peaks (E)
533 for *Tet1*$^{+/+}$, *Tet1*$^{HxD/HxD}$, and *Tet1*$^{-/-}$ prospermatogonia.

534 F-G) The significance of enrichment of TET1^{HxD}-rescued (F) or TET1^{HxD}-not rescued (G) DMRs
535 within regions where H3K4me3 was restored to WT levels in *Tet1*$^{HxD/HxD}$ prospermatogonia
536 following observed depletion in *Tet1*$^{-/-}$ prospermatogonia. In the graph, the grey-shaded region
537 under the curve represents the distribution of the number of overlaps between 1000 randomized
538 DMRs (within the array coverage) and the fixed set of H3K4me3-restored regions, values above
539 the red line correspond to the area with a significance of $p < 0.05$. The solid green line
540 represents the observed number of overlaps between rescued or not-rescued DMRs and
541 H3K4me3-restored regions. Z-scores represent the strength or standardized magnitude of
542 enrichment of overlap.

543

Barau J, Teissandier A, Zamudio N, Roy S, Nalesso V, Hérault Y, Guillou F, Bourc'his D. 2016. The DNA methyltransferase DNMT3C protects male germ cells from transposon activity. *Science* **354**: 909–912.

Barski A, Cuddapah S, Cui K, Roh T-Y, Schones DE, Wang Z, Wei G, Chepelev I, Zhao K. 2007. High-Resolution Profiling of Histone Methylations in the Human Genome. *Cell* **129**: 823–837.

Bourc'his D, Bestor TH. 2004. Meiotic catastrophe and retrotransposon reactivation in male germ cells lacking Dnmt3L. *Nature* **431**: 96–99.

Caldwell BA, Liu MY, Prasasya RD, Wang T, DeNizio JE, Leu NA, Amoh NYA, Krapp C, Lan Y, Shields EJ, et al. 2021. Functionally distinct roles for TET-oxidized 5-methylcytosine bases in somatic reprogramming to pluripotency. *Mol Cell* **81**: 859-869.e8.

Capotosti F, Guernier S, Lammers F, Waridel P, Cai Y, Jin J, Conaway JW, Conaway RC, Herr W. 2011. O-GlcNAc Transferase Catalyzes Site-Specific Proteolysis of HCF-1. *Cell* **144**: 376–388.

Chao L, Yang S, Li H, Long C, Xi Q, Zuo Y. 2022. Competitive binding of TET1 and DNMT3A/B cooperates the DNA methylation pattern in human embryonic stem cells. *Biochim Biophys Acta (BBA) - Gene Regul Mech* **1865**: 194861.

Chotalia M, Smallwood SA, Ruf N, Dawson C, Lucifero D, Frontera M, James K, Dean W, Kelsey G. 2009. Transcription is required for establishment of germline methylation marks at imprinted genes. *Genes Dev* **23**: 105–117. http://genesdev.cshlp.org/cgi/doi/10.1101/gad.495809.

Chrysanthou S, Tang Q, Lee J, Taylor SJ, Zhao Y, Steidl U, Zheng D, Dawlaty MM. 2022. The DNA dioxygenase Tet1 regulates H3K27 modification and embryonic stem cell biology independent of its catalytic activity. *Nucleic Acids Res* **50**: 3169–3189.

Clouaire T, Webb S, Skene P, Illingworth R, Kerr A, Andrews R, Lee J-H, Skalnik D, Bird A. 2012. Cfp1 integrates both CpG content and gene activity for accurate H3K4me3 deposition in embryonic stem cells. *Genes Dev* **26**: 1714–1728.

Dawlaty MM, Breiling A, Le T, Raddatz G, Barrasa MI, Cheng AW, Gao Q, Powell BE, Li Z, Xu M, et al. 2013. Combined deficiency of Tet1 and Tet2 causes epigenetic abnormalities but is compatible with postnatal development. *Dev Cell* **24**: 310–323. http://linkinghub.elsevier.com/retrieve/pii/S1534580712005898.

Deplus R, Delatte B, Schwinn MK, Defrance M, Méndez J, Murphy N, Dawson MA, Volkmar M, Putmans P, Calonne E, et al. 2013. TET2 and TET3 regulate GlcNAcylation and H3K4

579 methylation through OGT and SET1/COMPASS. *EMBO J* **32**: 645–655.
580 http://emboj.embopress.org/cgi/doi/10.1038/emboj.2012.357.

581 Dhayalan A, Rajavelu A, Rathert P, Tamas R, Jurkowska RZ, Ragozin S, Jeltsch A. 2010. The
582 Dnmt3a PWWP Domain Reads Histone 3 Lysine 36 Trimethylation and Guides DNA
583 Methylation*. *J Biol Chem* **285**: 26114–26120.

584 Erkek S, Hisano M, Liang C-Y, Gill M, Murr R, Dieker J, Schübeler D, Vlag J van der, Stadler
585 MB, Peters AHFM. 2013. Molecular determinants of nucleosome retention at CpG-rich
586 sequences in mouse spermatozoa. *Nat Struct Mol Biol* **20**: 868–875.

587 Ernst J, Kellis M. 2017. Chromatin-state discovery and genome annotation with ChromHMM.
588 *Nat Protoc* **12**: 2478–2492.

589 Ernst J, Kellis M. 2012. ChromHMM: automating chromatin-state discovery and
590 characterization. *Nat Methods* **9**: 215–216.

591 Fanourgakis G, Gaspa-Toneu L, Komarov PA, Papasaikas P, Ozonov EA, Smallwood SA, Peters
592 AHFM. 2025. DNA methylation modulates nucleosome retention in sperm and H3K4
593 methylation deposition in early mouse embryos. *Nat Commun* **16**: 465.

594 Gel B, Díez-Villanueva A, Serra E, Buschbeck M, Peinado MA, Malinverni R. 2015. regioneR:
595 an R/Bioconductor package for the association analysis of genomic regions based on
596 permutation tests. *Bioinformatics* **32**: 289–291.

597 Goodman RH, Smolik S. 2000. CBP/p300 in cell growth, transformation, and development.
598 *Genes Dev* **14**: 1553–1577.

599 Gu T, Lin X, Cullen SM, Luo M, Jeong M, Estecio M, Shen J, Hardikar S, Sun D, Su J, et al.
600 2018. DNMT3A and TET1 cooperate to regulate promoter epigenetic landscapes in mouse
601 embryonic stem cells. *Genome Biol* **19**: 88.
602 https://genomebiology.biomedcentral.com/articles/10.1186/s13059-018-1464-7.

603 Guenther MG, Levine SS, Boyer LA, Jaenisch R, Young RA. 2007. A chromatin landmark and
604 transcription initiation at most promoters in human cells. *Cell* **130**: 77–88.

605 Hanna CW, Taudt A, Huang J, Gahurova L, Kranz A, Andrews S, Dean W, Stewart AF,
606 Colomé-Tatché M, Kelsey G. 2018. MLL2 conveys transcription-independent H3K4
607 trimethylation in oocytes. *Nat Struct Mol Biol* **25**: 73–82.
608 http://www.nature.com/articles/s41594-017-0013-5.

609 Hill PWS, Leitch HG, Requena CE, Sun Z, Amouroux R, Roman-Trufero M, Borkowska M,
610 Terragni J, Vaisvila R, Linnett S, et al. 2018. Epigenetic reprogramming enables the transition
611 from primordial germ cell to gonocyte. *Nature* **555**: 392–396.
612 http://www.nature.com/doifinder/10.1038/nature25964.

613 Huang G, Liu L, Wang H, Gou M, Gong P, Tian C, Deng W, Yang J, Zhou T-T, Xu G-L, et al.
614 2020. Tet1 Deficiency Leads to Premature Reproductive Aging by Reducing Spermatogonia
615 Stem Cells and Germ Cell Differentiation. *iScience* **23**: 100908.

616 Huang Y, Sitwala K, Bronstein J, Sanders D, Dandekar M, Collins C, Robertson G, MacDonald
617 J, Cezard T, Bilenky M, et al. 2012. Identification and characterization of Hoxa9 binding sites
618 in hematopoietic cells. *Blood* **119**: 388–398.

619 Ito S, Shen L, Dai Q, Wu SC, Collins LB, Swenberg JA, He C, Zhang Y. 2011. Tet Proteins Can
620 Convert 5-Methylcytosine to 5-Formylcytosine and 5-Carboxylcytosine. *Science* **333**: 1300–
621 1303.

622 Joshi K, Liu S, S.J. PB, Zhang J. 2022. Mechanisms that regulate the activities of TET proteins.
623 *Cell Mol Life Sci* **79**: 363.

624 Kaneda M, Okano M, Hata K, Sado T, Tsujimoto N, Li E, Sasaki H. 2004. Essential role for de
625 novo DNA methyltransferase Dnmt3a in paternal and maternal imprinting. *Nature* **429**: 900–
626 903.

627 Kato Y, Kaneda M, Hata K, Kumaki K, Hisano M, Kohara Y, Okano M, Li E, Nozaki M, Sasaki
628 H. 2007. Role of the Dnmt3 family in de novo methylation of imprinted and repetitive
629 sequences during male germ cell development in the mouse. *Hum Mol Genet* **16**: 2272–2280.
630 https://academic.oup.com/hmg/article-lookup/doi/10.1093/hmg/ddm179.

631 Klobučar T, Kreibich E, Krueger F, Arez M, Pólvora-Brandão D, von Meyenn F, da Rocha ST,
632 Eckersley-Maslin M. 2020. IMPLICON: an ultra-deep sequencing method to uncover DNA
633 methylation at imprinted regions. *Nucleic Acids Res* **48**: gkaa567-.

634 Ko M, Bandukwala HS, An J, Lamperti ED, Thompson EC, Hastie R, Tsangaratou A, Rajewsky
635 K, Koralov SB, Rao A. 2011. Ten-Eleven-Translocation 2 (TET2) negatively regulates
636 homeostasis and differentiation of hematopoietic stem cells in mice. *Proc Natl Acad Sci USA*
637 **108**: 14566–14571. http://www.pnas.org/cgi/doi/10.1073/pnas.1112317108.

638 Kobayashi H, Sakurai T, Imai M, Takahashi N, Fukuda A, Yayoi O, Sato S, Nakabayashi K,
639 Hata K, Sotomaru Y, et al. 2012. Contribution of intragenic DNA methylation in mouse
640 gametic DNA methylomes to establish oocyte-specific heritable marks. ed. W. Reik. *PLoS*
641 *Genet* **8**: e1002440. https://dx.plos.org/10.1371/journal.pgen.1002440.

642 Kobayashi H, Sakurai T, Miura F, Imai M, Mochiduki K, Yanagisawa E, Sakashita A, Wakai T,
643 Suzuki Y, Ito T, et al. 2013. High-resolution DNA methylome analysis of primordial germ
644 cells identifies gender-specific reprogramming in mice. *Genome Res* **23**: 616–627.
645 http://genome.cshlp.org/cgi/doi/10.1101/gr.148023.112.

646 Kohli RM, Zhang Y. 2013. TET enzymes, TDG and the dynamics of DNA demethylation.
647 *Nature* **502**: 472–479. http://www.nature.com/doifinder/10.1038/nature12750.

648 Lauberth SM, Nakayama T, Wu X, Ferris AL, Tang Z, Hughes SH, Roeder RG. 2013. H3K4me3
649 Interactions with TAF3 Regulate Preinitiation Complex Assembly and Selective Gene
650 Activation. *Cell* **152**: 1021–1036.

651 Lee SM, Loo CE, Prasasya RD, Bartolomei MS, Kohli RM, Zhou W. 2024. Low-input and
652 single-cell methods for Infinium DNA methylation BeadChips. *Nucleic Acids Res* **52**: e38–
653 e38.

654 Lengner CJ, Camargo FD, Hochedlinger K, Welstead GG, Zaidi S, Gokhale S, Scholer HR,
655 Tomilin A, Jaenisch R. 2007. Oct4 expression is not required for mouse somatic stem cell
656 self-renewal. *Cell Stem Cell* **1**: 403–415.
657 https://linkinghub.elsevier.com/retrieve/pii/S1934590907000859.

658 Lian H, Li W-B, Jin W-L. 2016. The emerging insights into catalytic or non-catalytic roles of
659 TET proteins in tumors and neural development. *Oncotarget* **7**: 64512–64525.

660 Maezawa S, Sakashita A, Yukawa M, Chen X, Takahashi K, Alavattam KG, Nakata I, Weirauch
661 MT, Barski A, Namekawa SH. 2020. Super-enhancer switching drives a burst in gene
662 expression at the mitosis-to-meiosis transition. *Nat Struct Mol Biol* **27**: 978–988.

663 Molaro A, Hodges E, Fang F, Song Q, McCombie WR, Hannon GJ, Smith AD. 2011. Sperm
664 Methylation Profiles Reveal Features of Epigenetic Inheritance and Evolution in Primates.
665 *Cell* **146**: 1029–1041.

666 Ooi SKT, Qiu C, Bernstein E, Li K, Jia D, Yang Z, Erdjument-Bromage H, Tempst P, Lin S-P,
667 Allis CD, et al. 2007. DNMT3L connects unmethylated lysine 4 of histone H3 to de novo
668 methylation of DNA. *Nature* **448**: 714–717. http://www.nature.com/articles/nature05987.

669 Prasasya RD, Caldwell BA, Liu Z, Wu S, Leu NA, Fowler JM, Cincotta SA, Laird DJ, Kohli
670 RM, Bartolomei MS. 2024. Iterative oxidation by TET1 is required for reprogramming of
671 imprinting control regions and patterning of mouse sperm hypomethylated regions. *Dev Cell*
672 **59**: 1010-1027.e8.

673 Saitou M, Kagiwada S, Kurimoto K. 2011. Epigenetic reprogramming in mouse pre-implantation
674 development and primordial germ cells. *Development* **139**: 15–31.

675 Saitou M, Payer B, O'Carroll D, Ohinata Y, Surani MA. 2005. Blimp1 and the Emergence of the
676 Germ Line during Development in the Mouse. *Cell Cycle* **4**: 1736–1740.

677 SanMiguel JM, Abramowitz LK, Bartolomei MS. 2018. Imprinted gene dysregulation in a Tet1
678 null mouse model is stochastic and variable in the germline and offspring. *Development* **145**:
679 dev160622. http://dev.biologists.org/lookup/doi/10.1242/dev.160622.

680 Schneider R, Bannister AJ, Myers FA, Thorne AW, Crane-Robinson C, Kouzarides T. 2004.
681 Histone H3 lysine 4 methylation patterns in higher eukaryotic genes. *Nat Cell Biol* **6**: 73–77.

682 Seisenberger S, Andrews S, Krueger F, Arand J, Walter J, Santos F, Popp C, Thienpont B, Dean
683 W, Reik W. 2012. The dynamics of genome-wide DNA methylation reprogramming in mouse
684 primordial germ cells. *Mol Cell* **48**: 849–862.
685 http://linkinghub.elsevier.com/retrieve/pii/S109727651200932X.

686 Shirane K, Lorincz M. 2023. Epigenetic Mechanisms Governing Female and Male Germline
687 Development in Mammals. *Sex Dev* **16**: 365–387.

688 Shirane K, Miura F, Ito T, Lorincz MC. 2020. NSD1-deposited H3K36me2 directs de novo
689 methylation in the mouse male germline and counteracts Polycomb-associated silencing. *Nat*
690 *Genet* **52**: 1088–1098.

691 Singh P, Li AX, Tran DA, Oates N, Kang E-R, Wu X, Szabó PE. 2013. De novo DNA
692 methylation in the male germ line occurs by default but is excluded at sites of H3K4
693 methylation. *Cell Rep* **4**: 205–219.
694 https://linkinghub.elsevier.com/retrieve/pii/S2211124713002805.

695 Smith ZD, Meissner A. 2013. DNA methylation: roles in mammalian development. *Nat Rev*
696 *Genet* **14**: 204–220.

697 Stephens DC, Poon GMK. 2016. Differential sensitivity to methylated DNA by ETS-family
698 transcription factors is intrinsically encoded in their DNA-binding domains. *Nucleic Acids*
699 *Res* **44**: 8671–8681.

700 Stewart KR, Veselovska L, Kelsey G. 2016. Establishment and functions of DNA methylation in
701 the germline. *Epigenomics* **8**: 1399–1413. https://www.futuremedicine.com/doi/10.2217/epi-
702 2016-0056.

703 Stewart KR, Veselovska L, Kim J, Huang J, Saadeh H, Tomizawa S-I, Smallwood SA, Chen T,
704 Kelsey G. 2015. Dynamic changes in histone modifications precede de novo DNA
705 methylation in oocytes. *Genes Dev* **29**: 2449–2462.
706 http://genesdev.cshlp.org/lookup/doi/10.1101/gad.271353.115.

707 Vella P, Scelfo A, Jammula S, Chiacchiera F, Williams K, Cuomo A, Roberto A, Christensen J,
708 Bonaldi T, Helin K, et al. 2013. Tet proteins connect the O-linked N-acetylglucosamine
709 transferase Ogt to chromatin in embryonic stem cells. *Mol Cell* **49**: 645–656.
710 https://linkinghub.elsevier.com/retrieve/pii/S1097276512010556.

711 Williams K, Christensen J, Pedersen MT, Johansen JV, Cloos PAC, Rappsilber J, Helin K. 2011.
712 TET1 and hydroxymethylcytosine in transcription and DNA methylation fidelity. *Nature* **473**:
713 343–348. http://www.nature.com/articles/nature10066.

714 Wu H, D'Alessio AC, Ito S, Xia K, Wang Z, Cui K, Zhao K, Sun YE, Zhang Y. 2011. Dual
715 functions of Tet1 in transcriptional regulation in mouse embryonic stem cells. *Nature* **473**:
716 389–393. http://www.nature.com/articles/nature09934.

717 Xia B, Yan Y, Baron M, Wagner F, Barkley D, Chiodin M, Kim SY, Keefe DL, Alukal JP,
718 Boeke JD, et al. 2020. Widespread Transcriptional Scanning in the Testis Modulates Gene
719 Evolution Rates. *Cell* **180**: 248-262.e21.

720 Yamaguchi S, Hong K, Liu R, Shen L, Inoue A, Diep D, Zhang K, Zhang Y. 2012. Tet1 controls
721 meiosis by regulating meiotic gene expression. *Nature* **492**: 443–447.
722 http://www.nature.com/articles/nature11709.

723 Yamaguchi S, Shen L, Liu Y, Sendler D, Zhang Y. 2013. Role of Tet1 in erasure of genomic
724 imprinting. *Nature* **504**: 460–464. http://www.nature.com/articles/nature12805.

725 Yang C, Shapiro LH, Rivera M, Kumar A, Brindle PK. 1998. A Role for CREB Binding Protein
726 and p300 Transcriptional Coactivators in Ets-1 Transactivation Functions. *Mol Cell Biol* **18**:
727 2218–2229.

728 Zhang T, Murphy MW, Gearhart MD, Bardwell VJ, Zarkower D. 2014. The mammalian
729 Doublesex homolog DMRT6 coordinates the transition between mitotic and meiotic
730 developmental programs during spermatogenesis. *Development* **141**: 3662–3671.

731 Zhang Y, Jurkowska R, Soeroes S, Rajavelu A, Dhayalan A, Bock I, Rathert P, Brandt O,
732 Reinhardt R, Fischle W, et al. 2010. Chromatin methylation activity of Dnmt3a and
733 Dnmt3a/3L is guided by interaction of the ADD domain with the histone H3 tail. *Nucleic*
734 *Acids Res* **38**: 4246–4253.

735 Zhao J, Lu P, Wan C, Huang Y, Cui M, Yang X, Hu Y, Zheng Y, Dong J, Wang M, et al. 2021.
736 Cell-fate transition and determination analysis of mouse male germ cells throughout
737 development. *Nat Commun* **12**: 6839.

738 Zhu F, Zhu Q, Ye D, Zhang Q, Yang Y, Guo X, Liu Z, Jiapaer Z, Wan X, Wang G, et al. 2018.
739 Sin3a–Tet1 interaction activates gene transcription and is required for embryonic stem cell
740 pluripotency. *Nucleic Acids Res* **46**: 6026–6040.

741

742